



Effect of annealing on microstructure in railway wheel steel

Downloaded from: <https://research.chalmers.se>, 2025-12-05 03:12 UTC

Citation for the original published paper (version of record):

Nikas, D., Zhang, Y., Ahlström, J. (2022). Effect of annealing on microstructure in railway wheel steel. 42ND RISO INTERNATIONAL SYMPOSIUM ON MATERIALS SCIENCE: MICROSTRUCTURAL VARIABILITY: PROCESSING, ANALYSIS, MECHANISMS AND PROPERTIES, 1249. <http://dx.doi.org/10.1088/1757-899X/1249/1/012059>

N.B. When citing this work, cite the original published paper.

Effect of annealing on microstructure in railway wheel steel

Dimitrios Nikas^{1,2}, Yubin Zhang³ and Johan Ahlström^{1,*}

¹ Department of Industrial and Materials Science, Chalmers University of Technology, 412 96 Gothenburg, Sweden

² Department of Engineering and Physics, Karlstad University, 651 88 Karlstad, Sweden

³ Department of Civil and Mechanical Engineering, Technical University of Denmark, 2800 Kgs. Lyngby, Denmark

*E-mail: johan.ahlstrom@chalmers.se

Abstract. Railway wheels are commonly made from medium carbon steels (~0.55 wt.% C), heat treated to a near pearlitic microstructure with 5–10% pro-eutectoid ferrite. During the operation of freight trains, where block brakes are used, high thermal loads occur together with the high contact stresses, which combined can affect the mechanical properties of the material. In this study, the effects of annealing on local microstructure and mechanical properties in pearlitic railway wheel steel were investigated using electron microscopy and micro-hardness. It is found that after annealing at 650 °C, the room temperature hardness reduces about 25%, accompanied by significant spheroidization of cementite in the pearlitic colonies, though the size and the orientation gradients of the pearlitic colonies have not changed much. The relationship between the microstructural changes and the mechanical properties are discussed.

1. Introduction

Demands on railway wheels have increased in recent years due to the strive for higher train speeds for passenger transport and higher axle loads in freight operation. Especially freight wheels are exposed to very high temperatures in the wheel tread due to block braking systems exposing the wheel tread surface to frictional heating. The material in the tread of the wheel is also exposed to very high stresses from the rolling contact, resulting in cyclic plastic strains. Investigations presented in literature show that the temperature in the wheel tread can rise above 500 °C for wheels on freight trains [1]. Qualification tests of such wheels impose frictional heating of the wheel rim to around 600 °C imitating severe drag braking (50 kW, 45 minutes). This is done to ensure resistance against thermally induced radial cracks as well as to confirm that the shape of the wheel remains within limits necessary for the structural integrity (i.e. keeping the wheelset in shape for the rail gauge). Medium carbon steels (with approximately 0.55 wt.% C) are commonly used due to their cost-effective fatigue and wear properties, and because they can be reasonably well maintained under normal service conditions.

The manufacturing of railway wheels involves heat treatments in order to achieve desirable characteristics in mechanical properties and residual stress distributions. After heat treatments, the forged and rolled wheels have a running surface consisting of fine-lamellar pearlite, a structure of alternating hard cementite and softer ferrite lamellae with a lamellar spacing of around 130 nm, and



about 5-10% pro-eutectoid ferrite decorating the previous austenite grain boundaries [2,3]. The high temperatures occurring during operation can however degrade the microstructure, more specifically spheroidize the pearlitic microstructure. The effect of the microstructural degradation has been evaluated in previous studies and found to affect both the mechanical properties and the fatigue behavior [3,4]. Systematic studies of the microstructure after annealing at different temperatures are required to quantify the degradation process, information essential for optimization of the processing route and the mechanical properties of the pearlitic steel. It is also a necessity for accurate material modelling with a multi-scale approach, in order to describe the combined effects of thermal and mechanical loadings on orientation and microstructure degradation, yielding the strain and stress development for wheels in operation.

In this study, we use complementary characterization techniques, including optical microscopy (OM), Scanning Electron Microscopy (SEM) and Electron Back Scattered Diffraction (EBSD), to quantify the changes in microstructure after annealing of the pearlitic R8T steel grade used for railway wheels. With OM we can quantify the fraction of the pro-eutectoid ferrite covering a large area and characterize its morphology, while with SEM/EBSD we can characterize the changes in morphology of the pearlite and the crystallographic orientations within pearlite colonies. A previous study concerned pre-deformed wheel material representative of the near surface region, the first few millimeters below the surface, [5] while the current study concerns undeformed material at larger depths, which was exposed to only thermal loadings. The current study is connected to a parallel manuscript on Differential Aperture X-ray Microscopy (DAXM) done on the same material [6], and is supposed to provide the overview of the microstructure and the correlation to the mechanical properties. By characterization of material exposed to annealing treatments across different length scales, the overall picture of the degradation of pearlitic lamellar structure is obtained and becomes useful for multi-scale modelling of mechanical performance.

2. Material and experimental procedures

The material studied in this investigation is the railway wheel steel R8T which complies to the ER8 grade specified in the standard EN 13262-1. The manufacturing process of this wheel material consists of forging, rolling, heat treatment, rim chilling and annealing. Samples were extracted from unused ('virgin') wheels approximately 15 to 20 mm below the wheel tread surface; this material region is of interest since it will be exposed to elevated temperatures and mechanical loading during operation. Different heat treatments were done for the investigation, to provide a complete understanding of the annealing occurring during operation and enable setting suitable limits for use of the material. The experiments presented here concern virgin wheel material annealed for 4 hours at temperatures in the range 250 – 650 °C with an interval of 50 °C, but with the EBSD investigation focused on the cases also represented in the parallel DAXM study [6].

Vickers hardness values were measured before and after annealing for each sample using a Wolpert 2RC hardness tester and a load of 10 kg (HV10) with a dwell time of 12 s. Indents were positioned randomly on the sample surface and averaged based on three indents.

After heat treatment, the specimens were mechanically ground and polished down to 0.04 µm using a colloidal silica suspension. Gentle etching was done using Nital (3% HNO₃ in ethanol) to gain some topographical contrast. The EBSD measurements were carried out in a LEO 1550 high resolution field emission scanning electron microscope (FEG-SEM). The system was equipped with an EBSD detector (Nordlys, Oxford instruments), a high speed camera for EBSD pattern recording, and software for crystal orientation mapping (AZtechKL). The samples were tilted to 70° and the SEM was operating at an accelerating voltage of 20 kV. Crystallographic orientation maps were recorded within the pearlite colonies as well as within the pro-eutectoid ferrite, with a step size of 130 nm which is approximately the interlamellar spacing of the pearlite in this material [3]. This step size was chosen for mapping of large areas to resolve the orientation gradient within pearlite colonies, rather than resolve the local pearlitic structure. The material microstructure was evaluated in randomly chosen areas which were selected without focusing on any specific pearlite colony or other microstructural features.

Image analysis of SEM images was performed to quantify the degree of spheroidization at the various annealing temperatures. A Matlab script was developed to process SEM images for each sample at every temperature examined. The first step of the analysis was segmentation using a threshold value in brightness, to determine the areas corresponding to cementite and ferrite. A ‘thinning’ function was thereafter used to account for the sampling error resulting from cementite lamellae protruding after etching. The cementite areas were then separated into lamellar and globular cementite according to the length over width aspect ratio. Chattopadhyay and Sellars [7] state that regions with aspect ratios lower than 8 should be classified as globular. Using this definition and averaging the results from all (25) images for each sample, the percentage of lamellar and globular cementite was obtained for each temperature. A more detailed explanation of the method is available in [8]. An illustration of the division between lamellar and spheroidal cementite for a strongly spheroidised sample is shown in figure 1.

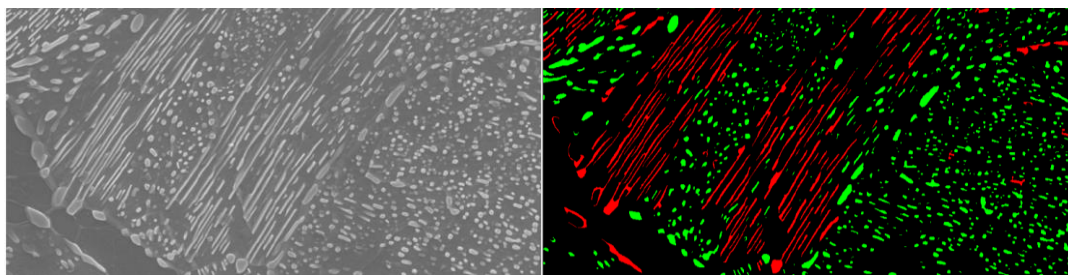


Figure 1. Degree of spheroidization determined from SEM images (from [8]). Original image on the left, processed image on the right (red regions are lamellar cementite defined as $L/W > 8$, green regions are defined as globular).

3. Results

The hardness of the virgin and the annealed samples are shown in figure 2a. The initial hardness of the R8T material in the virgin state is around 260 HV10. The material slightly hardens when annealing around 300 °C, whereas significant softening is observed for higher temperatures. The hardness decrease is approximately 25 % after 4 h annealing at 650 °C.

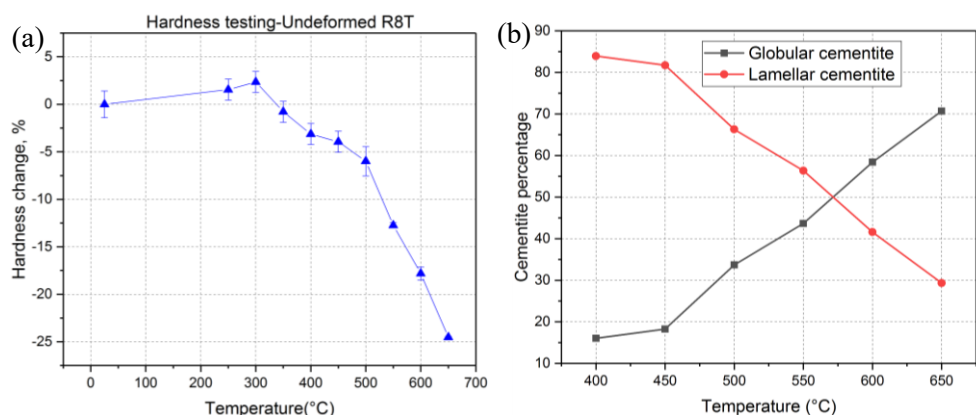


Figure 2. (a) Hardness change after annealing for 4 h relative to the virgin material. (b) Quantification of cementite spheroidization after annealing for 4 h.

The quantified cementite spheroidization fraction determined based on SEM images of the virgin and annealed samples are shown in figure 2b, and figure 3 shows SEM images for some of the examined temperatures. Below 400 °C, no noticeable change is seen in the pearlitic structure. The cementite lamellae start to break up at a temperature around 450 °C, while most of the pearlitic structure remains unchanged. By increasing the annealing temperature, cementite spheroidization becomes evident at 500 °C and gets severe at 650 °C, where ~70% of the cementite is globular (see figure 2b).

An SEM image and an inverse pole figure (IPF) EBSD map of the same field of view are shown in figure 4 for the sample annealed at 300 °C. Due to the small thickness of cementite lamellae, only a very small fraction of the cementite is indexed (~2%). Some grains containing many sub-grain boundaries in the EBSD map and with more contrast in the SEM image are likely pearlitic colonies (see for example the grain marked by P in figure 4a and b). The grains with uniform contrast in the SEM image and no sub-grain boundaries are generally pro-eutectoid ferrite (see for example the grain marked by F in figure 5a and b). Within the pearlite colonies long-range orientation gradients remain (see figure 4c).

Upon annealing at higher temperatures, 500 °C and 650 °C, the grain structures as observed in the EBSD maps do not change much (see figures 5 and 6), even though severe spheroidization of cementite lamellae occurs (figures 2b and 3d). The kernel average misorientation (KAM) map after annealing at 500 °C in figure 5c shows that the majority of the pearlitic colonies (see for example the grain marked by P in figure 5) still have large KAM values, while the pro-eutectoid ferrite grains have very low KAM values, $<0.5^\circ$ (see for example the grain marked by F in figure 5). At 650 °C, the orientation gradients in the ferrite within individual pearlite colonies only slightly redistribute locally (figure 6c), leading to well-defined cell boundaries (figure 6b top, marked P) and an increase in the measured fraction of low angle boundaries (see figure 7). The average low angle boundary spacing ($2\text{--}15^\circ$) changes slightly from 2.8 μm to 2.1 μm after annealing at 300 °C and 650 °C, respectively.

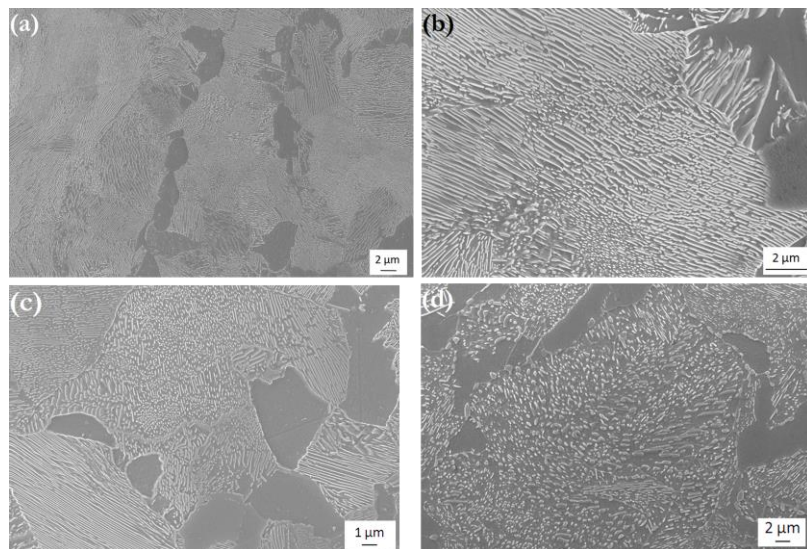


Figure 3. Microstructure of (a) virgin material, representative also for material annealed at 300 °C (b) annealed at 450 °C (c) annealed at 500 °C and (d) annealed at 650 °C. The annealing time was 4 h in all cases.

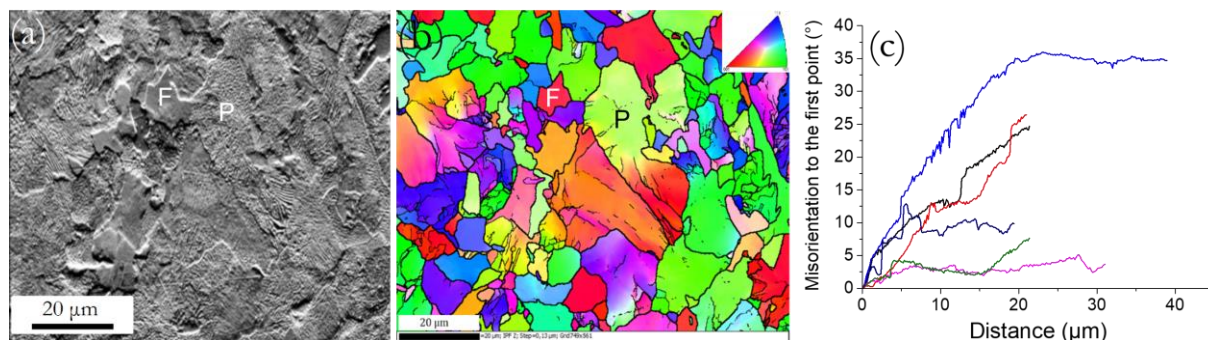


Figure 4. Microstructure and orientations in the sample annealed at 300 °C for 4 h. (a) SEM image, (b) IPF map, and (c) misorientation gradients within 6 randomly chosen pearlite grains. The colors in (b) represent the crystallographic orientation along the measured surface normal direction, see inset. The thin and thick black lines in (b) represent boundaries with misorientation angles $>2^\circ$ and $>10^\circ$, respectively. Letters F and P mark selected ferrite and pearlite grains, respectively.

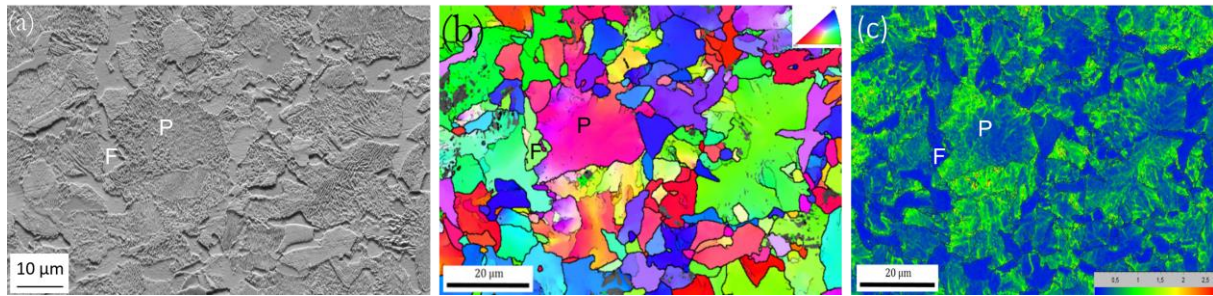


Figure 5. Microstructure and orientations in the sample annealed at 500 °C for 4 h. (a) SEM image, (b) IPF map. The colors in (b) represent the crystallographic orientation along the measured surface normal direction, see inset. (c) KAM map showing orientation variations within grains. KAM value for a given pixel is defined as the average misorientation angle of that pixel to its 8 nearest neighbors, calculated with the proviso that misorientation angles above a cut-off angle (3° for this map) are not counted in the averaging process.

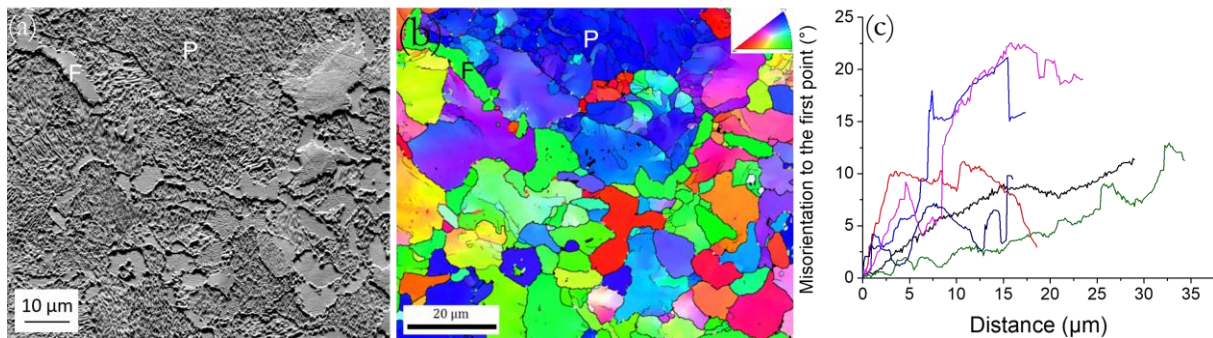


Figure 6. Microstructure and orientations in the sample annealed at 650 °C for 4 h. (a) SEM image, (b) IPF map, and (c) misorientation gradients within 6 randomly chosen pearlite grains. The colors in (b) represent the crystallographic orientation along the measured surface normal direction, see inset.

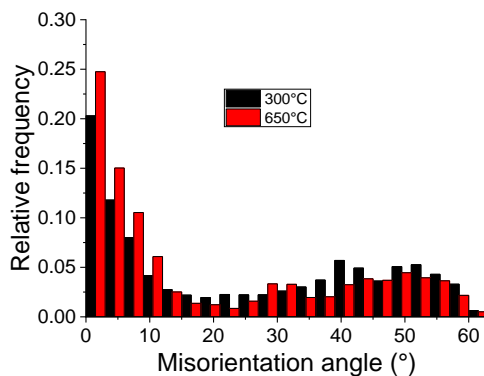


Figure 7. Distribution of misorientations between neighboring pixels of the annealed samples, determined based on the EBSD maps in figures 4 and 6 (step size of 130 nm).

4. Discussion

The results show that upon annealing the cementite lamellae start to break up at 450 °C in the pearlite colonies. Higher annealing temperatures lead to increasing degree of spheroidization. After annealing at 650 °C for 4 h, most of the pearlitic colonies have spheroidized (with cementite aspect ratio < 8). A sub-grain structure has formed in certain spheroidized pearlite colonies, but the long range orientation gradient within less spheroidized pearlite colonies does not change much even after annealing at 650 °C for 4 h. This is in agreement with previous studies reporting long-range orientation gradients remaining since the pearlite was formed in the eutectoid reaction [9]. Only localized changes in sub-

grain boundary spacing and morphology of the cells occur, which have a rather small effect on average values. This implies that even though the cementite lamellae break up and spheroidize, the neighboring ferrite lamellae re-orient only locally around the cell boundaries, and the total amount of geometrically necessary dislocations (GNDs) that produce the long range orientation gradient within the colonies does not reduce much. This is likely because the dislocations within the (connected) ferrite lamellae are pinned strongly due to the short free mean path between the spheroidized cementite particles and they cannot move long distances to reduce the long range orientation gradients.

Both the reduction in elastic strain and dislocation density may affect the mechanical properties. After annealing at 300 °C for 4h, part of the elastic strain [10] and some dislocations within the free ferrite grains are removed while the cementite and ferrite lamellae remain more or less unchanged. Both the reduction in elastic strain and dislocation density in the free ferrite grains should lead to a reduction of strength of the material, although the fraction of the free ferrite grains is only <10 %. However, this is not the case; the hardness of the annealed sample at 300 °C for 4 h instead increase about 2.5 % compared to the virgin sample. This is due to strain ageing which decreases the mobility of the dislocations [11]. Upon annealing at higher temperature, the elastic strain and dislocation density within the ferrite grains continue to decrease [6], and the cementite lamellae break up and spheroidise. In addition, the total dislocation density (both GNDs and statistically stored dislocations) within the pearlite colonies also reduces as the mean free path between cementite particles increases. All these factors contribute to reduce hardness and strength.

5. Summary

In the present study, the microstructure in annealed wheel steel samples were measured using electron backscatter diffraction in SEM. The microstructure of the unused railway wheel pearlitic steel, R8T, is quite stable upon annealing at 300 °C, while microstructural degradation in term of spheroidization of cementite lamellae in pearlite colonies occurs at temperatures higher than 450 °C. The size of the pearlitic colonies does not change much even after annealing at 650 °C for 4h, though ~70% of the cementite is spheroidized leading to large loss in hardness (-25%).

Acknowledgments

This work is part of the research activities within CHARMEC (Chalmers Railway Mechanics, www.charmec.chalmers.se). It was partly financed within the European Horizon 2020 research and innovation programme in the projects In2Track, In2Track2 and last in the In2Track3 project under grant agreement 101012456. YZ acknowledges the support by the European Research Council (ERC) under the European Union's Horizon 2020 research and innovation programme (grant No 788567, M4D).

References

- [1] Peters C J and Eifler D 2009 *Mater. Test.* **51** 748–54
- [2] Cvetkovski K, Ahlström J and Karlsson B 2011 *Wear* **271** 382–7
- [3] Nikas D, Ahlström J and Malakizadi A 2016 *Wear* **366–367** 407–15
- [4] Nikas D and Ahlström J 2014 *Proceedings of the 35th Risø international symposium of material science*, Eds S. Faester, et al. pp 411-420
- [5] Nikas D and Ahlström J 2015 *IOP Conf. Series: Mater. Sci. Eng.* **89**
- [6] Zhang Y, Jessop C, Nikas D, Yu T, Liu W and Ahlström J 2022 submitted to *42nd Risø international symposium of material science*
- [7] Chattopadhyay S and Sellars C M 1977 *Metallography* **10** 89–105
- [8] Nikas D 2018 PhD thesis Chalmers Univ Tech
- [9] Takahashi T, Ponge D and Raabe D 2007 *Steel Res. Int.* **78** 38–44
- [10] Yildirim C, Jessop C, Ahlström J, Detlefs C, and Zhang Y 2021 *Scr. Mater.* **197** 113783
- [11] Baird J D 1971 *Metall. Rev.* **16** 1–18